JOURNAL OF CATALYSIS **169,** 55–66 (1997)
ARTICLE NO. CA971647

SAPO-11, SAPO-31, and SAPO-41 Molecular Sieves: Synthesis, Characterization, and Catalytic Properties in *n*-Octane Hydroisomerization

P. Mériaudeau,[1] V. A. Tuan, V. T. Nghiem, S. Y. Lai, L. N. Hung, and C. Naccache

Institut de Recherches sur la Catalyse, CNRS, 2 Av. Albert Einstein, 69626 Villeurbanne Cedex, France

Received November 25, 1996; revised January 20, 1997; accepted January 20, 1997

Large-pore SAPO-5 and medium-pore SAPO-11, SAPO-31, and SAPO-41 have been synthesized using a hydrothermal method. These catalysts were characterized by chemical analysis, XRD, SEM, IR, TPD of NH_3, and MAS NMR; Pt dispersion was measured by H_2 adsorption. *n*-Octane hydroconversion over the Pt–SAPO catalysts has been tested. High selectivity for *n*-octane isomerization has been observed on medium-pore Pt–SAPO-11, -31, and -41, while preferential hydrocracking has been found for large-pore Pt–SAPO-5. Isomerization products consisted of monobranched isomers with a negligible amount of dibranched isomers. Interestingly, among the medium-pore SAPOs, SAPO-41 exhibits the highest isomerization selectivity. The selectivity decreases in the order SAPO-41 > SAPO-31 > SAPO-11. The differences in isomerization selectivities of the SAPOs are explained by considering diffusional restriction and steric constraints, SAPO-41 channel dimensions adequately fitting the dimensions of the monobranched isomers.

© 1997 Academic Press

INTRODUCTION

The hydroisomerization of *n*-paraffins is of considerable interest and plays an important role in the petroleum industry. The branching of *n*-paraffins is needed to improve the octane number of gasoline and to increase the low-temperature performance of diesel.

Bifunctional catalysts containing a hydrogenating function and an acid function have shown high efficiency in isomerizing *n*-paraffins. However, the isomerization reaction is always accompanied by a hydrocracking reaction which lowers more or less the yield of isomerized feed molecules. It is well established that isomerization of *n*-alkanes occurs first and cracking is a consecutive reaction which is favored for multibranched alkanes; monobranched paraffins are less susceptible to cracking than multibranched paraffins (1, 2). Thus in order to decrease cracking reactions it was necessary to limit multibranching by employing shape-selective zeolite catalysts (3) or by favoring the desorption from the acid sites of the monobranched methylcarbenium intermediates (4).

Recently catalysts highly selective for the hydroisomerization of long-chain *n*-paraffins (5, 6) have been described. These catalysts are composed of medium-pore silicoaluminophosphate molecular sieves containing platinum (or palladium). SAPO-11, with a monodimensional pore system which consists of nonintersecting elliptical 10-membered ring pores of diameter 0.39×0.63 nm, was found most suitable for obtaining high yield isomerization of long-chain *n*-alkanes (5–7). Bifunctional 10-membered nonintersecting channels ZSM-22 with cross section 0.45×0.55 nm also exhibit high selectivity for isomerization of long-chain alkanes with the predominant formation of 2- and 3-methyl isomers (3).

In the present work we studied in detail the behavior of three medium-pore nonintersecting channel silicoaluminophosphate molecular sieves, SAPO-11, SAPO-31, and SAPO-41. These materials differ from each other by small differences in the 10-membered cross section, the proton acidity strength being almost the same. As indicated above, SAPO-11 has one-dimensional 10-membered ring channels with an elliptical pore opening of 0.39×0.63 nm.

SAPO-31 has circular monodimensional channels 0.54×0.54 nm in diameter; SAPO-41, a new medium-pore SAPO type (its framework topology has recently been determined (8)), has a unidimensional elliptical 10-membered ring pore 0.43×0.70 nm in diameter. In fact the 10-membered rings in SAPO-41 are not strictly elliptical and furthermore are slightly larger in size than the elliptical 10-membered ring in SAPO-11.

Due to differences in pore sizes and shapes it was expected that more or less peculiarities in the hydroconversion of *n*-alkanes would be observed. The synthesis and characterization of SAPO-11, SAPO-31, and SAPO-41 have been performed and the catalysts for the hydroconversion of *n*-octane have been obtained by supporting platinum on these SAPO materials.

[1] Corresponding author.

0021-9517/97 $25.00
Copyright © 1997 by Academic Press
All rights of reproduction in any form reserved.

For a basis of comparison, large-pore SAPO-5 has also been investigated.

EXPERIMENTAL

SAPO-11, -31, and -41 were hydrothermally synthesized using pseudo-boehmite (Catapal B, Vista), orthophosphoric acid (85%, Fluka), silica sol (Ludox AS 40), and dipropylamine (Fluka) as template. In the case of SAPO-5 tripropylamine or triethylamine was used. The synthesis gels were prepared as follows: pseudo-boehmite was added to the mixture of orthophosphoric acid and water with vigorous stirring at room temperature for 4 h until the gel was homogeneous. The template was added followed by silica sol with stirring and the resulting mixture was stirred for 2 h until it was homogeneous. These mixtures were transferred into stainless-steel autoclaves lined with PTFE, heated in an oven to 200°C, and then left at this temperature for 24 h. The synthesis products were washed, dried at 120°C for 3 h, and then calcined at 600°C for 40 h in air in order to remove the template completely. Metal loading was carried out by wet impregnation with $Pt(NH_3)_4Cl_2$. After impregnation for 24 h, the materials were dried at 120°C and finally calcined in flowing O_2 at 320°C for 20 h and reduced in flowing H_2 at 500°C for 2 h.

Products were characterized by X-ray powder diffraction (XRD; Philips W 1050 powder diffractometer) using Cu$K\alpha$ radiation, scanning electron microscopy (SEM; HITACHI S 800), and infrared spectroscopy (IR; Perkin–Elmer 580 Fourrier transform infrared spectrometer). Chemical compositions were determined by atomic absorption. Acidity of the samples was characterized by using temperature-programmed desorption of ammonia (TPD) of NH_3. ^{27}Al, ^{29}Si, and ^{31}P MAS NMR spectra were recorded at ambient temperature with a Bruker DSX 400 multinuclear spectrometer. Spin speeds were ca. 5.5 kHz (^{29}Si) and 12 kHz (^{27}Al and ^{31}P). The resonance frequencies observed were 79.5 MHz (^{29}Si), 104.2 MHz (^{27}Al), and 161.9 MHz (^{31}P). Chemical shifts were recorded with respect to TMS for ^{29}Si, $[Al(H_2O)_6]^3$ for ^{27}Al, and H_3PO_4 for ^{31}P.

Pt metal dispersion was determined by H_2 adsorption using a classical volumetric apparatus. The Pt dispersion was calculated by assuming that each Pt surface atom chemisorbs one hydrogen atom.

The catalytic conversion of *n*-octane was carried out in a fixed-bed continuous-flow microreactor at temperatures ranging from 200 to 400°C, under atmospheric pressure, at an $H_2/n\text{-}C_8$ molar ratio of 54, and at hourly space velocities ranging from 0.4 to 7 h^{-1}. Reaction products were analyzed by gas chromatography. The chromatographs were equipped with a capillary column (Pona, from Altech, France) and with a Bentone column (Altech, France).

Prior to starting the reaction, the catalysts (0.01–0.1 g) were treated *in situ* in the microreactor in flowing hydrogen whereby the temperature was increased up to 400°C. Subsequently, the temperature was decreased to the desired reaction temperature.

RESULTS AND DISCUSSION

Preparation of SAPOs

Medium-pore SAPO-11, -31, and -41 were hydrothermally synthesized using dipropylamine as template.

SAPO-11

SAPO-11 was synthesized according to the U.S. patent (9) with the following molar gel composition:

Template	Al_2O_3	P_2O_5	SiO_2	H_2O
2.0	1.0	1.0	0.1	50

SAPO-11 was crystallized at 200°C and the crystallization time was 24 h.

SAPO-31

Synthesis of SAPO-31 is more difficult. Attempts to crystallize SAPO-31 as described in the U.S. patent (10) were not successful. Only SAPO-11 or amorphous materials were obtained. Some modifications of the gel composition proposed in (11) have been done. Well-crystallized SAPO-31 was obtained using the following gel composition:

Template	Al_2O_3	P_2O_5	SiO_2	H_2O
1.0	1.2	1.0	0.6	50

The condition of crystallization of SAPO-31 is also limited. SAPO-31 crystallized at a relatively high temperature (200°C) and in a short time (24 h). Prolongation of crystallization time leads to cocrystallization of SAPO-11.

SAPO-41

Syntheses of AlPO-41 and Me-AlPO-41 have been patented (10). Attempts based on this patent to substitute Si for P and/or Al were not successful.

Only SAPO-11 or an unknown structure was obtained. The gel composition and the conditions of crystallization to obtain pure SAPO-41 have been systematically investigated. A typical gel composition for synthesis of SAPO-41 was found. SAPO-41 is well crystallized with the following molar composition:

Template	Al_2O_3	P_2O_5	SiO_2	H_2O
3.0	0.85	1.0	0.1	50

The gel was crystallized in an autoclave at 200°C for 24 h.

SAPO-5

To study the influence of pore size on catalytic properties, large-pore SAPO-5 was synthesized. Like SAPO-11, SAPO-5 crystallizes with a wide range of gel compositions and in a wide range of temperatures. In this study, SAPO-5 was crystallized with the following gel composition (template: triethylamine or tripropylamine):

Template	Al_2O_3	P_2O_5	SiO_2	H_2O
2.0	1.0	1.0	0.4	50

The crystallization was performed in a Teflon-lined stainless-steel autoclave at 200°C for 24 h.

Characterization of SAPOs

Chemical Composition

The chemical compositions of the gel and the solid products are given in Table 1. Based on the data listed in Table 1 it is concluded that the crystallized SAPO solids have almost the same composition as the corresponding gel. However, in the case of SAPO-31 the introduction of a high Si content in the gel leads to the incomplete conversion of Si to the crystallized product. Only ca. 60% of Si is converted into crystalline SAPO-31.

Interestingly, in the case of SAPO-41, a redistribution of the composition between gel and solid product is noted. A lower content of P and a higher content of Si in the solid product than in the gel are observed. This suggests a high degree of substitution of Si for P in the $AlPO_4$ framework.

Structure and Morphology of SAPOs

XRD. The X-ray powder diffraction patterns of the as-synthesized SAPO-5, -11, -31, and -41 are shown in Fig. 1. The position and intensity of the lines are identical to those reported for SAPO-5, -11, -31, and -41 (10, 12). No additional lines for each structure are observed, indicating that the samples are almost free of impurity. The high intensity of the XRD lines and the low background in the XRD pattern indicate high crystallinity of the samples.

SEM. The scanning electron micrographs of the samples are shown in Fig. 2. A different morphology is observed for each SAPO. The crystal form is of polycrystalline aggregates with sizes from 5 to 20 μm. They are composed of small crystallites of 0.5 to 1.5 μm. The crystal size distribution in the SAPO samples are not uniform and they differ from each other.

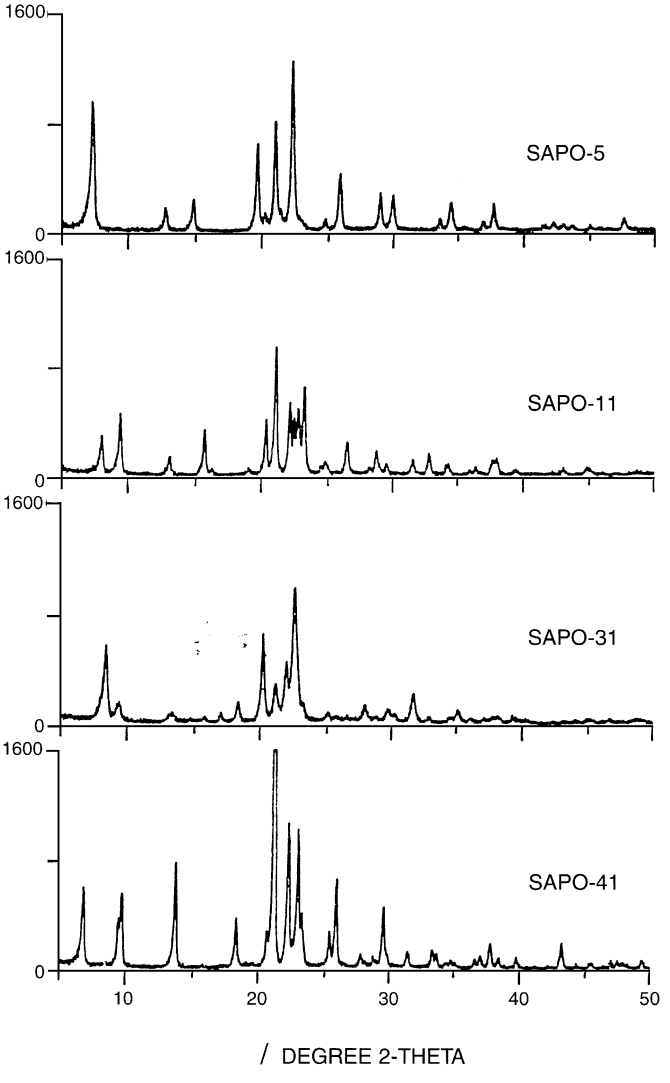

FIG. 1. X-ray diffraction patterns of SAPO-5, SAPO-11, SAPO-31, and SAPO-41.

TABLE 1

Chemical Composition of Gel and Solid Product in SAPO-11, SAPO-31, and SAPO-41

	Gel (wt%)			Solid product (wt%)		
SAPO	Al	P	Si	Al	P	Si
SAPO-11	21.60	24.80	1.12	21.24	24.10	1.22
SAPO-31	21.57	20.64	5.59	21.10	22.67	3.28
SAPO-41	19.56	26.40	1.19	21.25	23.72	1.72

MAS NMR. The ^{27}Al MAS NMR spectra of the samples are given in Fig. 3. The ^{27}Al MAS spectra show a sharp resonance centered at 36 ppm from tetrahedrally coordinated aluminum ion bound via oxygen to four P atoms (13). A small downfield resonance at ca. 10 ppm is observed, which is most probably caused by octahedrally coordinated aluminum atoms of unreacted starting material (14). Especially in the case of SAPO-31, the intensity of this line at 10 ppm is relatively high, indicating that the SAPO-31 sample contains a certain amount of extra-framework aluminum. Thus, higher Al content in the gel composition of SAPO-31 then in the compositions of other SAPOs (11 and

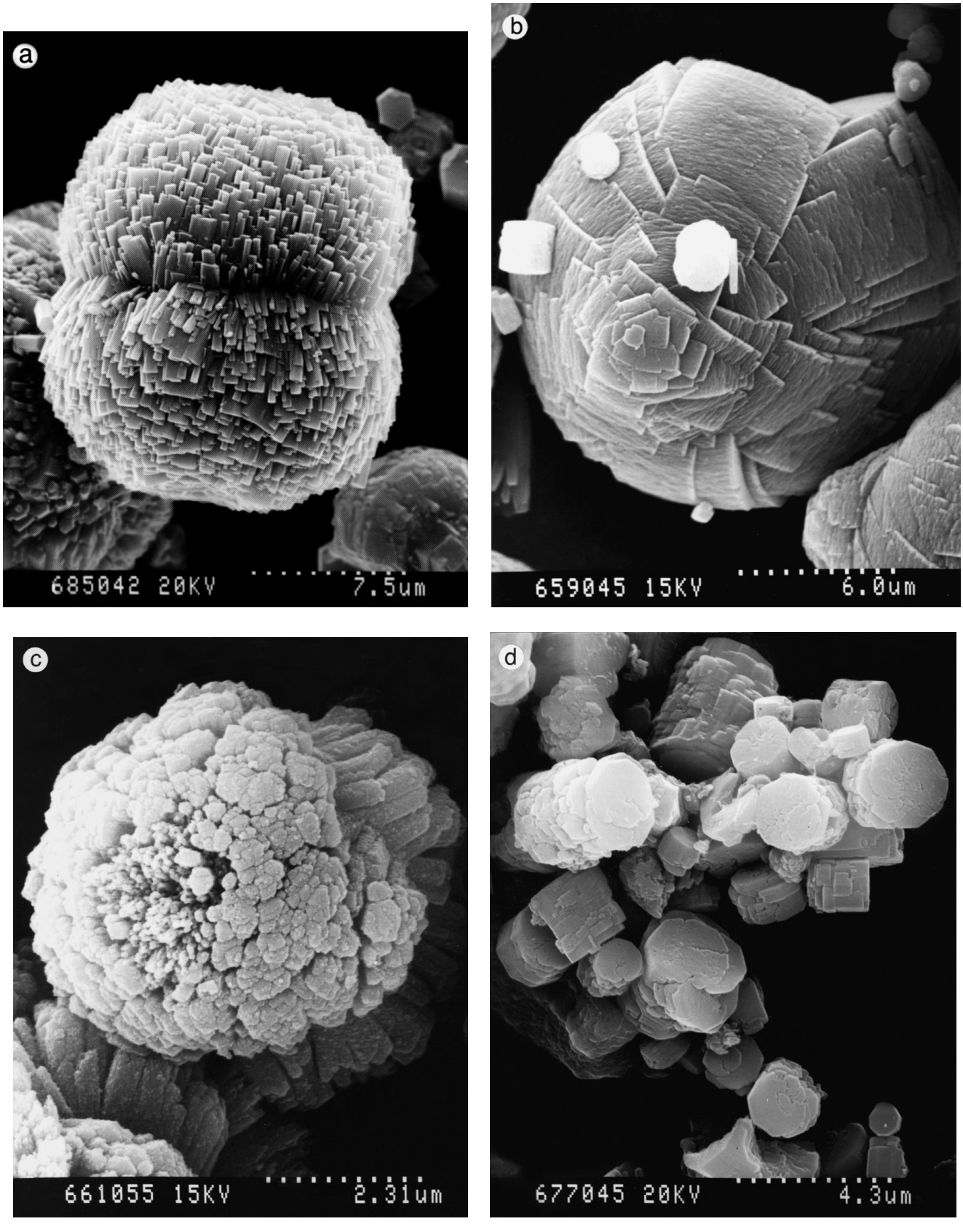

FIG. 2. Scanning electron micrographs of (a) SAPO-5, (b) SAPO-11, (c) SAPO-31, and (d) SAPO-41.

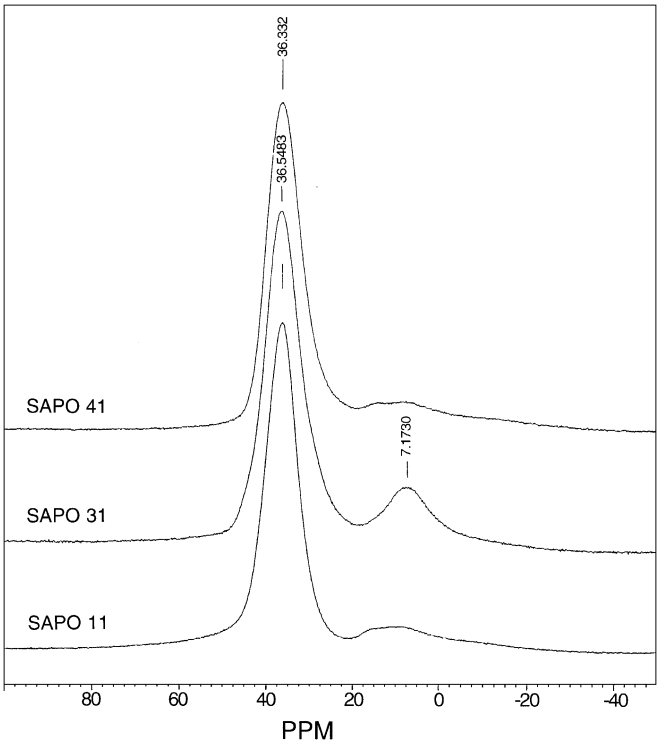

FIG. 3. ^{27}Al MAS NMR spectra of SAPO-11, SAPO-31, and SAPO-41.

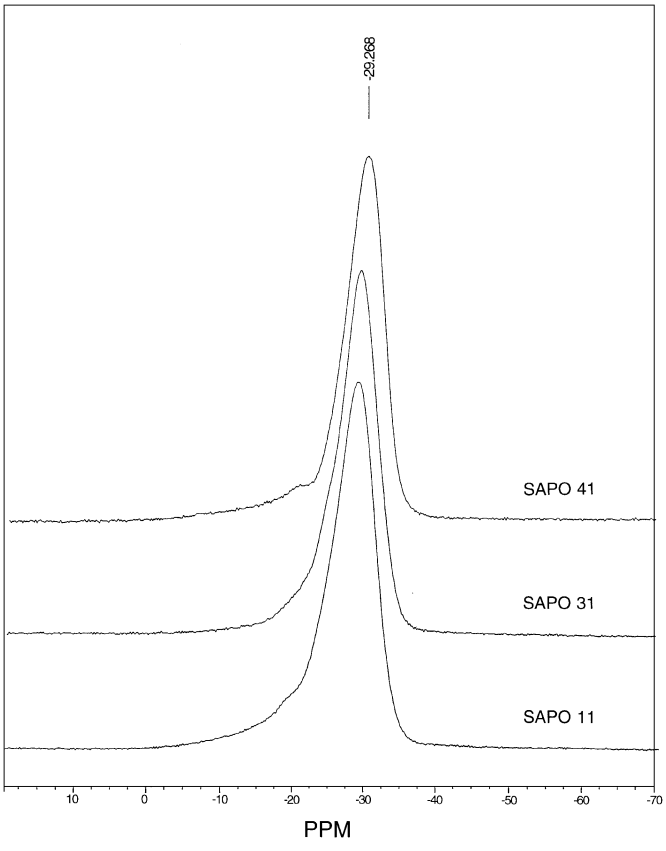

FIG. 4. ^{31}P MAS NMR spectra of SAPO-11, SAPO-31, and SAPO-41.

41) may lead to the incorporation of only a part of the aluminum ion into the framework, the other part remaining in the form of aluminum oxide.

The ^{31}P NMR spectra of the samples are shown in Fig. 4. The ^{31}P MAS spectra show one single sharp line at −29 ppm, assigned to Q tetrahedral P site with neighboring AlO_4 tetrahedral P(4Al) (15). A small additional line at −23 ppm in all samples is also observed. The slight shift of this line toward the value of the free phosphoric acid may suggest that these P sites are not fully linked to four AlO_4 tetrahedra, but to three AlO_4 and one OH. The ^{31}P MAS resonance at −23 ppm should be attributed to P($3AlO_4$, 1Al−OH) groups (16).

The ^{29}Si MAS NMR spectra of the samples are shown in Fig. 5.

Resonances centered around −91 and −96 ppm are observed. These resonances are ascribed to tetrahedral silicon atoms bound via oxygen to four aluminum atoms [Si (4Al)] (17). Consequently, the silicon present in the samples is almost incorporated on phosphorus T sites of the aluminophosphate framework. Each Si atom incorporated in this way should produce a Brønsted acidic site.

For the samples with low Si content, the predominant line at −93 ppm in the ^{29}Si NMR spectra is observed, which implies that the substitution of a single Si for a single P predominates (Figs. 5a and 5b). For the samples with higher Si content, the additional line at −110 ppm is noted. The line is consistent with Si atoms linked to neighboring Si

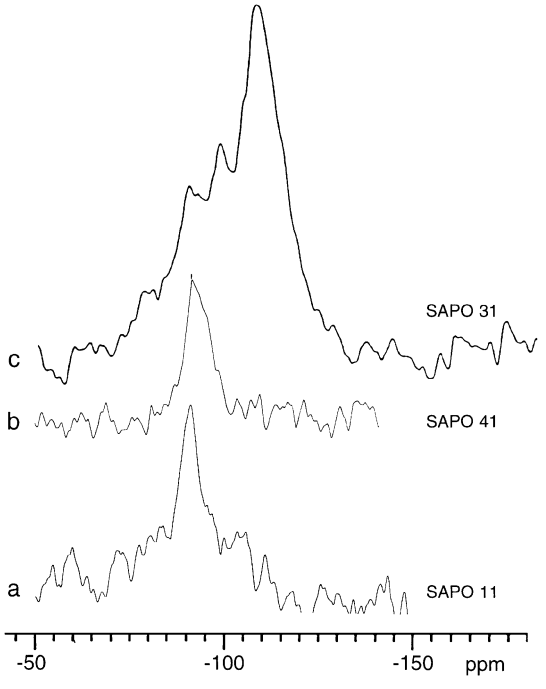

FIG. 5. ^{29}Si MAS NMR spectra of SAPO-11, SAPO-31, and SAPO-41.

atoms, i.e., a siliceous crystal domain (18). This reflects a combination of the substitution of a single Si for a single P and two Si for one Al and one P (19). For the samples with high Si content, the predominant line at −110 ppm (Fig. 5c) is observed, which implies that the substitution of two Si for one Al and one P predominates, a siliceous domain being formed. The ^{29}Si MAS NMR spectrum of SAPO-31 shows an intense signal at −110 ppm which may also be assigned to Si(4Si) in one silica–alumina domain (18). However, since the overall acidity of SAPO-31 is found to be relatively low compared to that of SAPO-11 and SAPO-41, one should conclude that a heterogeneous Si distribution has occurred in SAPO-31; only a pure siliceous rather than a SA domain was formed.

Acidity of SAPOs

IR. The nature and quantity of hydroxyl groups generated by Si incorporation were studied by IR. The spectra of the samples in the OH-stretching vibration domain are shown in Fig. 6. In the spectra of all SAPO samples, three bands at ca. 3743, 3677, and 3625 cm^{-1} are observed. The bands at 3743 and 3677 cm^{-1} are assigned to the Si–OH and P–OH groups on the external surface (20). The band at ca. 3625 cm^{-1} is attributed to the Brønsted acid site of the Si(OH)Al group (20, 21). In the case of SAPO-5, an additional band at ca. 3570 cm^{-1} is observed. This band can be attributed to OH bridged groups interacting with the oxygen atoms of the framework (22). Our results indicate that the frequency of the IR band corresponding to acidic Si(OH)Al groups was slightly dependent on the type of SAPO samples.

In addition, it was found that the intensity of these IR bands increased with the increased degree of replacement of P with Si.

It is observed that the intensity of the IR band around 3625 cm^{-1} in SAPO-41 and SAPO-11 is much larger than that in SAPO-31. The chemical analysis and ^{29}Si MAS NMR data show that SAPO-31 possesses the highest Si content and that the substitution of two Si for one Al and one P predominates with respect to the substitution of one P by one Si. These results along with the IR data clearly indicate that the number of Brønsted acid sites generated by Si substitution depends not only on the Si content but also mainly on the mechanism of Si substitution in the $AlPO_4$-framework.

TPD of NH_3. Further information about the number and strength of acid sites can be obtained by TPD of NH_3. TPD profiles of NH_3 for the samples are plotted in Fig. 7. The TPD curves showed two peaks for all SAPO samples. A low-temperature peak at ca. 180–200°C and a high-temperature peak at ca. 300–320°C correspond respectively to the desorption of NH_3 from weak acid sites and from strong acid sites (23). In the case of SAPO-5, the position of the high-temperature maximum is approximately 30°C lower than that observed for SAPO-11, -31, and -41. The shift of the high-temperature maximum cannot necessarily be related to differences in the acid strength of sites. This might be caused by the influence of the individual pore width and structure of the void volume of the different types of molecular sieves on the diffusion of the desorbing ammonia molecules. Indeed, small-pore SAPOs (SAPO-17 and SAPO-34) showed the high-temperature maximum shifted to ca. 50–70°C higher temperature than that observed for SAPO-11, -31, and -41 (23, 24). The high-temperature peak in the TPD profiles of SAPOs is much lower (ca. 100–150°C) in comparison to silicoaluminate zeolites, indicating their relatively lower acidity. Among SAPO samples, the strength of strong acid sites seems to be similar. However, the distribution of acid sites is different. The distribution of

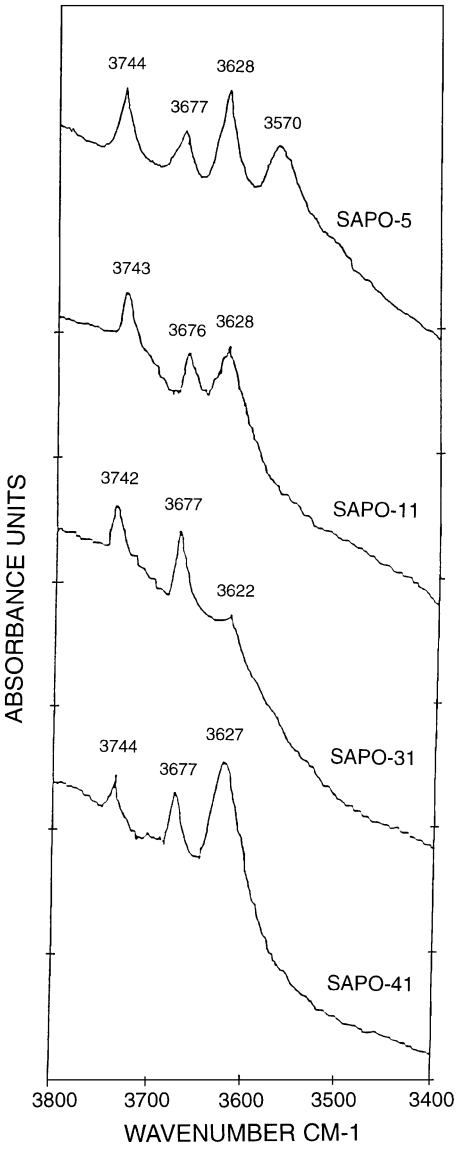

FIG. 6. IR spectra of hydroxyl groups in SAPO-5, SAPO-11, SAPO-31, and SAPO-41.

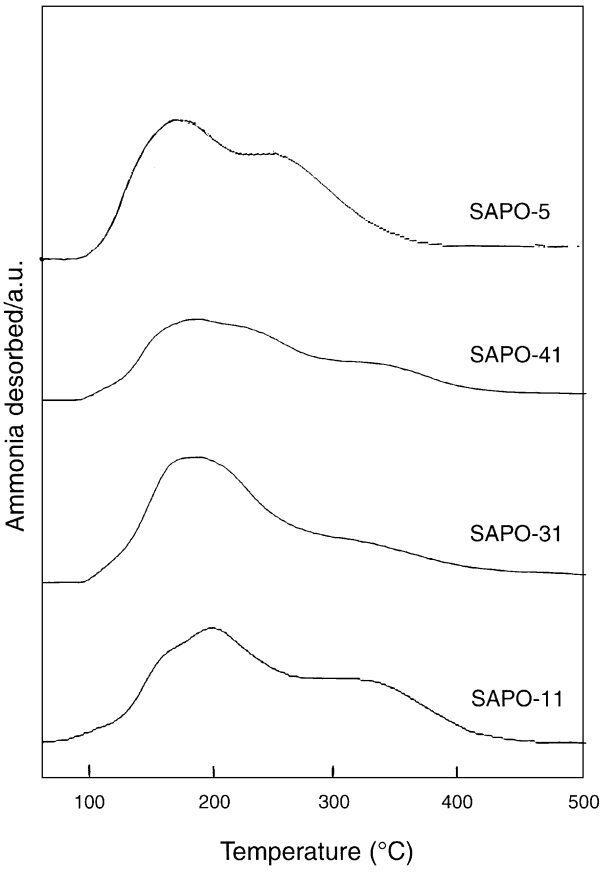

FIG. 7. TPD of NH_3 curves of SAPO-5, SAPO-11, SAPO-31, and SAPO-41.

acid sites and the intensity of acidic OH groups are given in Table 2.

From the IR and TPD studies, it could be concluded that the strength of the strong acid sites of the different SAPOs is similar to but lower than that of the aluminosilicate molecular sieves. Also the distribution of weak and strong acid sites depends on the mode fo Si substitution, the formation of Si–O–Si domains leading to a reduced acidity. The number of strong acid sites of SAPOs synthesized in this work decreased in the order SAPO-41 > SAPO-11 > SAPO-31.

TABLE 2

Determination of the Amount of Acid Sites of Different SAPOs by TPD of NH_3 and IR

Samples	Acidity (mmol NH_3/g solid) (TPD of NH_3)			Acidic OH group intensity (by IR, a.u.)
	Weak acid sites (100–250°C)	Strong acid sites (250–420°C)	Total amount	
SAPO-11	0.41	0.29	0.70	0.073
SAPO-31	0.60	0.18	0.78	0.045
SAPO-41	0.86	0.37	1.23	0.086
SAPO-5	0.46	0.36	0.82	0.075

Metal Dispersion

The metal dispersion of the catalysts determined by hydrogen adsorption is given in Table 3. The different SAPO samples were loaded with 1 wt% platinum. From this table it is clear that a relatively high Pt dispersion was obtained over the different SAPO supports, and furthermore almost similar Pt dispersion was observed in all the samples.

n-Octane Hydroconversion

The two major reactions occurring were isomerization and cracking. Figure 8 shows *n*-octane conversion as a function of the reaction temperature for the different Pt–SAPO catalysts under the same reaction conditions. Pt–SAPO-5 exhibited the highest catalytic activity. It is remarkable that the high catalytic hydroconversion activity of Pt–SAPO-5 was also accompanied by a high cracking activity.

Among the other medium-pore SAPO samples, Pt–SAPO-41 was the most active. The hydroconversion activity decreases in the order SAPO-41 > SAPO-11 > SAPO-31.

As stated above, and considering that the Pt content (1 wt%) and the high Pt dispersion (around 65%) are sufficient to provide the dehydrogenation activity required to balance the acidity of the catalysts, the hydroconversion activities of the different Pt–SAPOs must, in principle, be essentially governed by the acidity.

Table 2 shows that, except for SAPO-31, the different SAPO materials exhibit almost identical acid site number and acid site strength. Hence one should expect that SAPO-5, SAPO-41, and SAPO-11 will give almost similar catalytic activities in the hydroconversion of *n*-octane.

The results shown in Fig. 8 contrast significantly with these expectations, indicating that the catalytic activity over SAPO-based bifunctional catalysts is not influenced only by the acidity. The SAPO-5, SAPO-41, SAPO-31, and SAPO-11 frameworks contain monodimensional channels and no cages. The pore structure of SAPO-5 is a cylinder with a 12-membered ring of 0.73-nm cross section.

SAPO-41 channels have an elliptical 10-membered aperture of cross section 0.7×0.43 nm, and SAPO-11 channels have 10-membered elliptical pores of cross section 0.63×0.39 nm. Within these one-dimensional pore structures the diffusivity of the molecules will thus be considerably affected by the cross section of the pores. Within the channels of SAPO-41 and SAPO-11 the more restricted space as compared with the space available in SAPO-5

TABLE 3

Pt Dispersion Measured by H_2 Adsorption

	SAPO-5	SAPO-11	SAPO-31	SAPO-41
Pt dispersion (%)	75	70	55	64

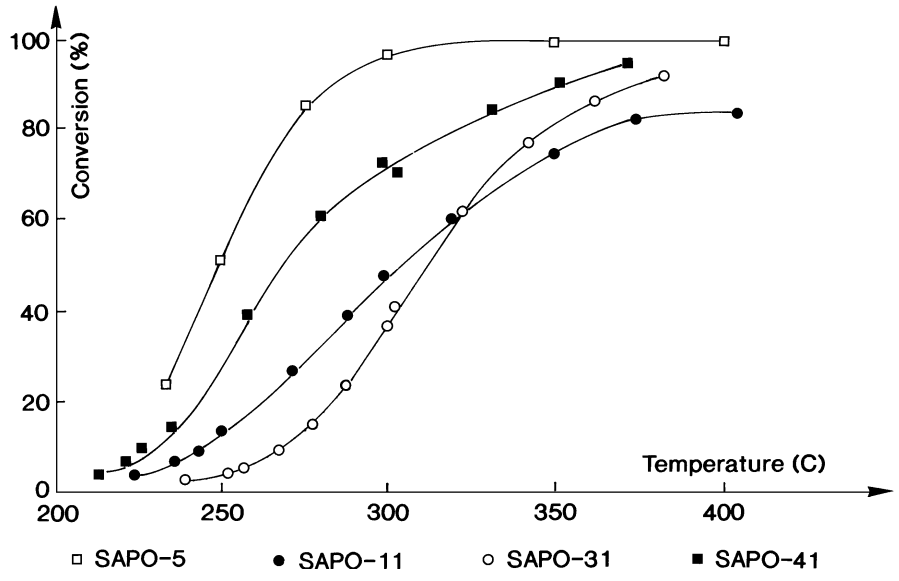

FIG. 8. *n*-Octane conversion as a function of temperature for SAPO-5, SAPO-11, SAPO-31, and SAPO-41.

channels causes a greater hindrance in the diffusion of *n*-octane-isomerized products. Thus the hydroconversion rate of *n*-octane over SAPO-41 and SAPO-11, due to a greater diffusion limitation, is less than that obtained over large-pore SAPO-5.

Over medium-pore SAPO catalysts, such as SAPO-41, SAPO-31, and SAPO-11, and reaction rate will be even more controlled by the diffusion. Among the three solids, SAPO-11, with the smallest pore size, will exhibit the highest diffusional limitation rate control and hence the lowest reaction rate in *n*-octane conversion as long as the catalysts show identical acidity. The constraint in SAPO-41 being less than that in SAPO-11 as a result of its slightly larger pore size explains the higher conversion observed with SAPO-41 than with SAPO-11.

SAPO-31 has the lowest acidity among the different SAPOs studied. The low activity of SAPO-31 is thus explained by the combined effects of diffusion limitation and low acidity.

Selectivities

Curves representing the yields of *n*-octane isomers versus the conversion are shown in Fig. 9. The increase of *n*-octane conversion was obtained by increasing the

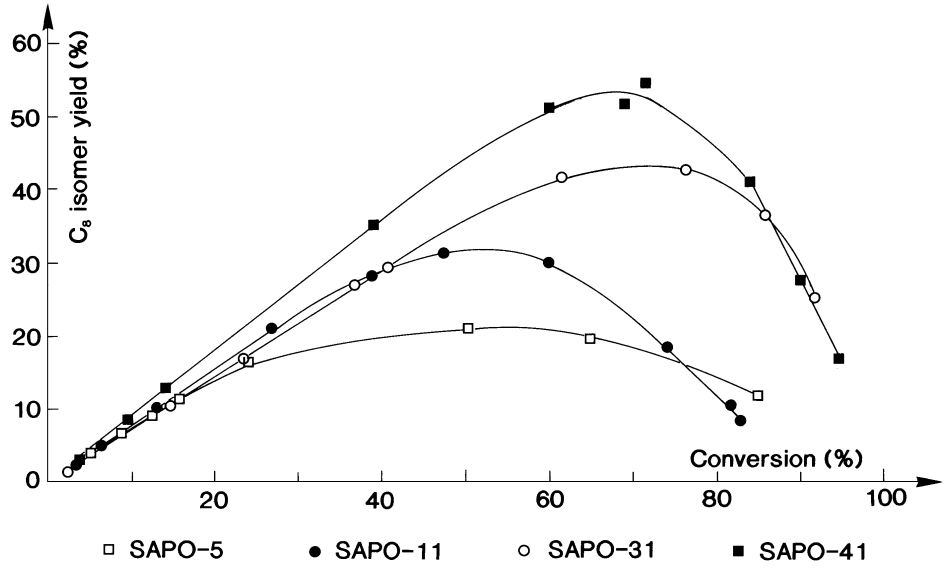

FIG. 9. Isomerization conversion of *n*-octane as a function of the total conversion of *n*-octane with different SAPOs.

reaction temperature within the range 220–380°C, the other experimental parameters being unchanged. These curves clearly show that as expected from the bifunctional mechanism, isomerization and cracking are consecutive reactions, iso-C_8 being the only reaction product obtained at low conversion. These results exclude the possibility of a direct cracking of the feed.

Figure 9 indicates that the C_8 isomer yields go through a maximum, the height and the position of the maximum isomer yield depending on the SAPO structure. The highest C_8 isomer yield was obtained with Pt–SAPO-41, approximately 65%. The efficiency of the various Pt–SAPO catalysts in yielding iso-C_8 decreased in the order

Pt–SAPO-41 > Pt–SAPO-31 > Pt–SAPO-11 > Pt–SAPO-5.

With large-pore SAPO-5, at low conversion (less than 20%), *n*-octane isomerization was the main reaction, similar to the behavior of the other medium-pore SAPO catalysts. However, at higher conversion hydrocracking became predominant, *n*-octane being cracked predominantly at the central position. In addition, high selectivity for branched cracked products is obtained, the molecular ratios iC_4/n_4 and iC_5/nC_5 being higher than 1. These results indicate, as already proposed by others (6), that over large-pore Pt–SAPO-5, due to the absence of geometric constraints within the channels, multibranched C_8 isomers such as dimethylhexyl and trimethylpentyl carbenium ions can be formed, which are rapidly cracked via β-scission, the cracking of the tribranched carbenium ions favoring central cracking of the hydrocarbon chain and also favoring branched cracked products.

The Respective Roles of Acid Strength and Porosity

The hydroisomerization and hydrocracking reactions over bifunctional catalysts depend generally on the relative strength of the hydrogenation and acid functions. The acidity of the different medium-pore SAPOs used in this work was not much different from one sample to another except that SAPO-5 has fewer acid sites. The hydrogenation activity was almost identical over these samples. Hence the different selectivity for *n*-octane isomerization (Fig. 9) and for cracking (Fig. 10) over SAPO-41, SAPO-31, and SAPO-11 must be ascribed, as already proposed for Pt–SAPO-11 (7), to steric constraint by the narrow pores of these solids, which restricts the formation of multibranched C_8-carbenium ion intermediates, these intermediates being rapidly cracked at high temperature, while the cracking of monobranched alkenyl carbenium ions is a relatively slow process.

Therefore, the difference in cracking activity over Pt–SAPO-11, -31, and -41 should originate from the structure effects. The size of the pores, as well as the size and the shape of the space available near the acid sites, can thus determine to a large extent the selectivity of *n*-octane transformation in bifunctional Pt–SAPO catalysts.

Among medium-pore SAPOs, SAPO-11 has a smaller pore size and a more elliptical pore opening than SAPO-41 and SAPO-31. This can be related to a slower migration of the intermediate alkenes and would ensure a longer contact time between the alkene and the acid sites, favoring consecutive transformation into cracking products. The diffusional behavior will also be related to configurational influences.

Qualitative predictions of the diffusion of molecules in medium-pore zeolites can be made by comparing the critical molecular diameters (25). This is defined as the smallest

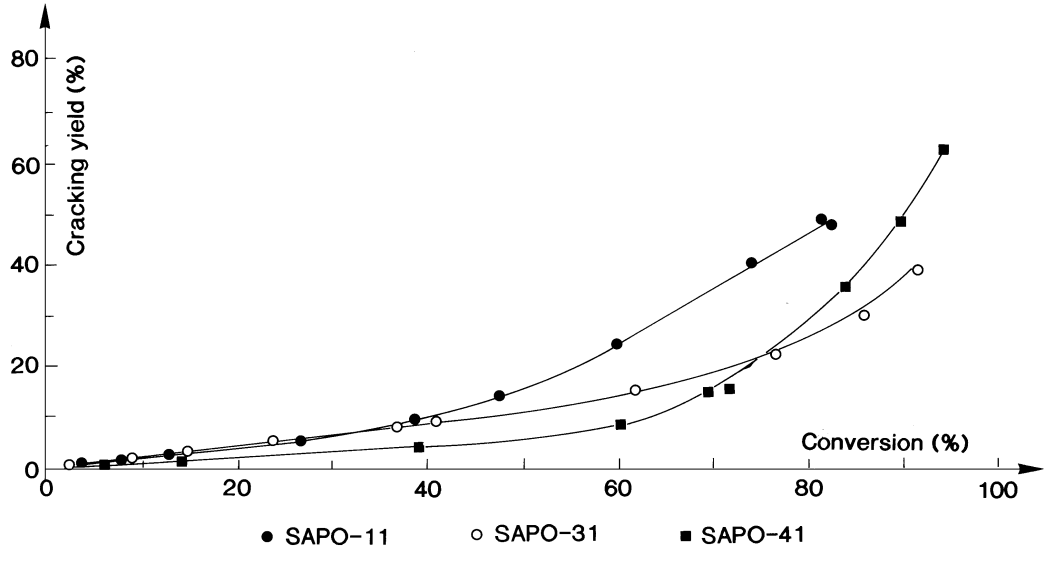

FIG. 10. Cracking conversion of *n*-octane as a function of the total conversion of *n*-octane with different SAPOs.

cylinder which can enclose the molecule in its most favorable equilibrium configuration.

The different isomerization selectivities within the SAPO series can be understood as a result of differences in their pore dimensions which impose differences in the residence times of the reaction intermediates in the channels. The critical molecular diameters are 0.49 nm for *n*-octane, 0.56 nm for monobranched MeC_7, and 0.7 nm for dibranched C_8 isomers. Comparison of these molecular diameters with channels of SAPO-11 (0.39×0.63 nm), SAPO-31 (0.54×0.54 nm), and SAPO-41 (0.43×0.7 nm) clearly indicates that the diffusional restriction is lower for SAPO-41 and SAPO-31. Over SAPO-41, with the less restricted pore size, monomethyl, and to a lesser extent dimethyl C_8 isomers would diffuse out of the channels more rapidly than when SAPO-31 and even more when SAPO-11 was involved. It results that the residence time of monobranched methylcarbenium ions for sterical reasons will be less over SAPO-41 and hence preferential desorption of monobranched C_8 isomers will occur rather than β-scission and/or additional branching. Within the more restricted channels of SAPO-31 and SAPO-11, a longer residence time of the monobranched C_8 isomers accounts for these monobranched carbenium ions being either cracked or further isomerized into dibranched intermediates which crack faster than monobranched carbenium ions. The results of the longer residence time of the intermediates within the SAPO-11 channels will be lower isomerization selectivity and larger amounts of branched cracking products. It is remarkable that a subtle change of the pore geometry and pore size of medium-pore SAPO series modifies the efficiency of these catalysts significantly toward the isomerization of long-chain alkanes. SAPO-41 showed the best apparent performance in *n*-octane hydroisomerization.

The isomerization activities of the three medium-pore SAPO catalysts were compared at a low reaction temperature in order to minimize the cracking reaction. The comparison was made for a reaction temperature of 300°C and at an *n*-octane conversion level of 50% by varying the space velocity of the feed. The results are given in Table 4. This table shows again that SAPO-41 is the most selective hydroisomerization catalyst. Typically the selectivity decreased in the order SAPO-41 > SAPO-31 > SAPO-11.

All these medium-pore SAPOs gave a high yield of monobranched 2-methylheptane and 3-methylheptane, but again the selectivity toward monomethylheptane decreased in the order SAPO-41 > SAPO-31 > SAPO-11.

At the 50% conversion level of *n*-octane the amount of dimethylhexanes was low over the medium-pore SAPO samples and furthermore an almost identical amount of dimethylhexanes was formed over these samples. High isomerization selectivity resulted for the medium-pore SAPO-41, SAPO-31, and SAPO-11 because the formation of multibranched carbenium ions, which are very sensitive to β-scission, was inhibited within the restricted pore volume (Fig. 11). It is likely that the most important cracking mechanism over these samples involves β-scission of monobranched and dibranched C_8 isomers. The predominantly formed 2-methylheptyl-4 and 3-methylheptyl-5 account for the formation of linear cracking products.

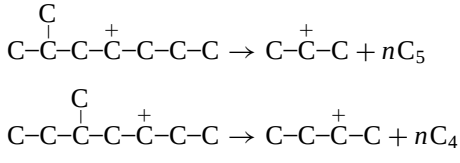

The molecular ratio $(C_3 + C_5)/2C_4$ being approximately 1, the absence of a significant amount of branched cracked products observed with Pt–SAPO-41 at 50% conversion (Table 4) can be understood as a result of the above β-scission of monobranched heptyl cations. The dimethyl carbenium ions would also crack into branched fragments but the small number of such dimethylhexenyl cations formed at 50% conversion on SAPO-41 accounts for the near absence of branched C_4 and C_5 isomers.

One could suggest that within the channels of SAPO-41, the 2-methylheptane and 3-methylheptane would desorb fast enough to avoid subsequent branching of the linear chain. The main hydrocracking mechanism, at this conversion level, involves monomethyl-branched carbenium ions with a minor contribution of the cracking of dimethyl-branched carbenium ions. By contrast, over SAPO-31 and SAPO-11, central cracking of the *n*-octane chain predominated over nonsymmetrical β-scission and furthermore substantial amounts of iso-C_4 and iso-C_5 were formed. These results indicate that the cracking of dibranched dimethylhexyl carbenium ions participated to an important extent in the overall cracking mechanism over SAPO-31 and SAPO-11. This work has shown conclusively that the product distributions of the *n*-octane reaction on SAPO are controlled by the pore size of the catalysts, large-pore SAPO-5 favoring the cracking reaction. The interpretations given in this paper are essentially based on "diffusion-controlled shape selectivity." However, it is worthwhile to consider the

TABLE 4

Isomerization of *n*-Octane over Pt–SAPO, $T = 300$°C, Conversion 50%

Sample	Selectivity[a] Iso-C_8[b]	Selectivity[a] MeC_7[c]	$3MeC_7/2MeC_7$	$DMeC_6/MeC_7$	$(C_3+C_5)/2C_4$	iC_4/nC_4	iC_5/nC_5
SAPO-41	94	88	0.80	0.07	1	0.01	0.01
SAPO-31	84	80	0.86	0.05	0.64	0.53	0.26
SAPO-11	80	73	0.87	0.09	0.75	0.3	0.29

[a] Carbon basis.
[b] All C_8 isomers.
[c] Monomethyl C_7.

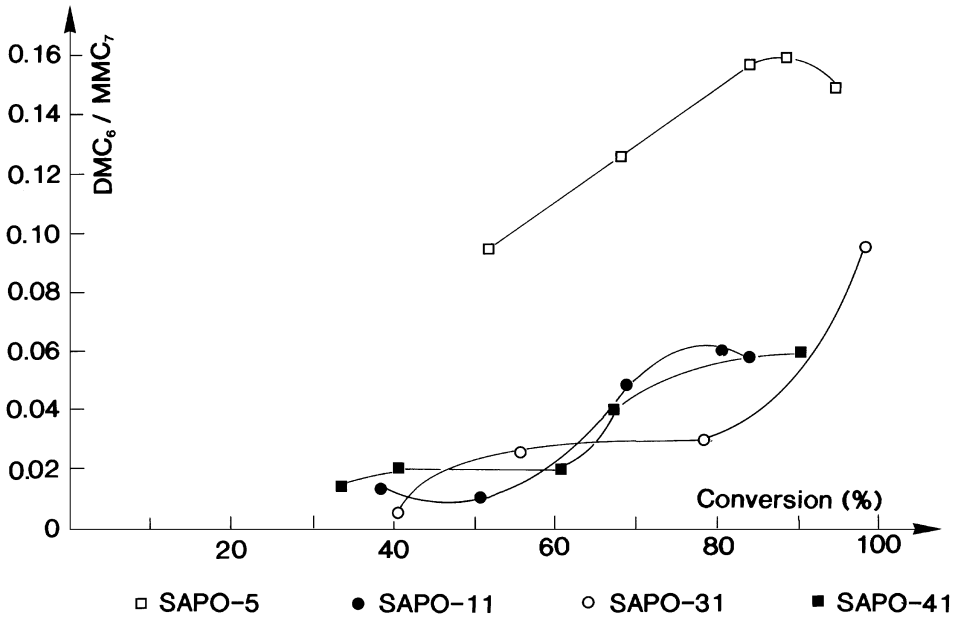

FIG. 11. Distribution of isomerized products (ratio of dibranched C_8/monobranched C_8) as a function of the degree of *n*-octane conversion with different SAPOs.

concepts developed by Martens *et al*. (26), who suggested that selective isomerization of long-chain alkanes occurred on active sites present in interrupted cavities and in pore mouths at the external surface of narrow-pore zeolites. The authors have nicely explained the preferential formation of monobranched alkanes at the terminal position using the pore mouth catalysis concept and the formation of di- and multibranched isomers at positions determined by the distance between neighboring pore months by the "key-lock" concept (27). It is not clear how these concepts could apply to *n*-octane isomerization since in 2,5- or 2,4-dimethylhexane isomers the branched methyl groups are separated by only two methylene carbon atoms. Nevertheless further work is in progress to evaluate the relative contribution of pore mouth catalysis and intracrystalline catalysis in the isomerization of C_8 alkanes.

CONCLUSION

Large-pore SAPO-5 and medium-pore SAPO-11, -31, and -41 were successfully synthesized using the hydrothermal method. In particular, the optimal gel composition and crystallization conditions for the synthesis of SAPO-41 were determined. The synthesized products are highly crystalline and not contaminated with impurities.

From NMR and other characterizations, it was shown that Si substitution in the medium-pore $AlPO_4$ framework occurred according to two mechanisms:

—One Si atom substitutes for one P atom.
—Two Si atoms substitute for one P atom and for one Al atom, depending on the gel composition and synthesis conditions.

The substitution of silicon atoms for phosphorus T sites in the $AlPO_4$ framework leads to the formation of Brønsted sites.

Medium-pore SAPOs possess medium acid strength. The strength of these acid sites in different SAPOs seems to be similar, but their density is different, depending on the Si content and the nature of Si substitution. The number of acid sites of SAPO samples decreases in the order SAPO-41 > SAPO-11 > SAPO-31.

In *n*-octane hydroconversion, preferential hydrocracking has been found for large-pore Pt–SAPO-5 , while preferential isomerization has been observed on medium-pore Pt–SAPO-11, -31, and -41. The observed high activity and selectivity of these catalysts in isomerization are due to their unique combination of mild acidity and shape selectivity.

Interestingly, among the medium-pore SAPOs, SAPO-41 exhibits the highest isomerization selectivity. The selectivity decreases in the order SAPO-41 > SAPO-31 > SAPO-11. The difference in isomerization selectivity of SAPOs could be explained by diffusional restriction and by steric constraints; the size and shape of the channels in SAPO-41 adequately fit those of the monobranched isomers, allowing fast desorption of the isomerization products instead of substantial cracking.

ACKNOWLEDGMENT

The authors thank the European Commission (Contract C11-CT93-0361) for financial support.

REFERENCES

1. Martens, J. A., Jacobs, P. A., and Weitkamp, J., *Appl. Catal.* **20**, 239 (1986).
2. Martens, J. A., Tielen, M., and Jacobs, P. A., *Stud. Surf. Sci. Catal.*, 46 (1989).
3. Ernst, S., Weitkamp, J., Martens, J. A., and Jacobs, P. A., *Appl. Catal.* **48**, 137 (1989).
4. Parton, R., Uytterhoeven, L., Martens, J. A., Jacobs, P. A., and Froment, G., *Appl. Catal.* **76**, 131 (1991).

5a. Miller, S. J., U.S. Patent 5,135,638 (1992).

5b. Miller, S. J., *Microporous Mater.* **2**, 439 (1994).

6. Taylor, R. J., and Petty, R. H., *Appl. Catal. A* **119**, 121 (1994).
7. Campelo, J. M., Lafont, F., and Marinas, J. M., *J. Catal.* **156**, 11 (1995).
8. Kirchner, R. M., and Bennett, J. M., *Zeolites* **14**, 523 (1994).
9. Wilson, S. T., Lok, B. M., and Flanigen, E. M., U.S. Patent 4310440 (1982).
10. Lok, B. M., Messina, C. A., Patton, R. I., Gajek, R. T., Cannan, T. R., and Flaningen, E. M., U.S. Patent 4440871 (1984).
11. Zubowa, H. L., Alsdorf, E., Fricke, R., Neissendorfer, F., Richter-Mendau, J., Schreïer, E., Zergan, D., and Zibrowius, B., *J. Chem. Soc. Faraday Trans.* **86**, 2307 (1990).
12. Brent, M. L., Celeste, A. M., Patton, R. I., Gajek, R. T., Cannan, T. R., and Flaningen, E. M., Eur. Patent 103,117 (1982).
13. Müller, D., Gessner, W., Samoson, A., Lippmaa, E., and Scheler, G., *J. Chem. Soc. Dalton Trans.*, 1277 (1986).
14. Jahn, E., Müller, D., Wieker, W., and Richter-Mendau, M., *Zeolites* **9**, 177 (1989).
15. Müller, D., Jahn, E., Ladwig, G., and Haubenreisser, U., *Chem. Phys. Lett.* **109**, 332 (1984).
16. Jahn, E., Müller, D., and Becker, K., *Zeolites* **10**, 15 (1990).
17. Blackwell, C. S., and Patton, R. L., *J. Phys. Chem.* **92**, 3965 (1988).
18. Martens, J. A., Grobet, P. J., and Jacobs, P. A., *J. Catal.* **126**, 299 (1990).
19. Ojo, A. F., Dwyer, J., Dewing, J., O'Malley, P. J., and Nabhan, A., *J. Chem. Soc. Faraday Trans.* **88**, 105 (1992).
20. Wilson, S. T., Lok, B. M., Messina, C. A., Cannan, T. R., and Flanigen, E. M., *Am. Chem. Soc. Symp. Ser.* **218**, 79 (1983).
21. Hedge, S. G., Ratnasamy, P., Kustov, L. M., and Kazansky, V. B., *Zeolites* **8**, 137 (1988).
22. Zibrowius, B., Löffler, E., and Hunger, M., *Zeolites* **12**, 167 (1992).
23. Parlitz, B., Schreier, E., Zubowa, H. L., Eckelt, R., Lieske, E., Lischke, G., and Fricke, R., *J. Catal.* **155**, 1 (1995).
24. Schnabel, K. H., Fricke, R., Girnus, I., Jahn, E., Löffler, E., Parlitz, B., and Peuker, C., *J. Chem. Soc. Faraday Trans.* **87**, 3569 (1991).
25. Choudhary, V. R., and Akolekar, D. B., *J. Catal.* **117**, 542 (1989).
26. Martens, J. A., Souverijns, W., Verrelst, W., Parton, R., Froment, G. F., and Jacobs, P. A., *Angew. Chem. Int. Ed. Engl.* **34**, 2528 (1995).
27. Souverijns, W., Martens, J. A., Uytterhoeven, L., Froment, G. F., and Jacobs, P. A., *in* "Progress in Zeolite and Microporous Materials" (H. Chon, S. K. Ihm, and Y. S. Uh, Eds.), Studies in Surface Science and Catalysis, Vol. 105, p. 1285. Elsevier, Amsterdam/New York, 1997.